

Feedback Control of a Soft Swinging Appendage

Travis Burch¹, John P. Lathrop², William L. Scott³, Derek A. Paley⁴

Abstract—This paper presents a state-space description using planar discrete elastic rod theory of a soft robotic appendage with torque input at one end. We design a linear output feedback controller to balance the appendage in an unstable vertical configuration with an angle sensor and torque input collocated at the base. Gains are tuned through simulations of the nonlinear system and hardware experiments are performed to verify performance. Simulation results suggest that the resulting control design balances some appendages that would otherwise buckle under their own weight.

I. INTRODUCTION

Robotic systems designed with soft components have decreased weight, size, and mechanical complexity as compared to traditional rigid robots [1]. Soft robots have been used in many tasks, including gripping delicate objects [2], as well as in underwater locomotion [3]. However, soft and flexible systems are challenging to model because they may be highly nonlinear, have infinite degrees of freedom, and are generally described by partial differential equations [4]. Much of the existing literature in the field of flexible manipulators focuses on relatively stiff structures with sufficiently well-defined vibration modes, which can be modeled with the Assumed Modes Method (AMM) [5]. However, existing models break down when soft materials such as silicone rubber undergo large deformations [5]. In this case, state-space modeling and principled control design is possible using elastic rod theory [6].

As a representative problem, this paper considers the stabilization of a soft appendage mounted on a rotating base with a torque input as shown in Fig. 1. The nonlinear behavior and complexity of existing models that describe the dynamics of flexible beams complicate traditional control design [7]. Prior work has been done in modeling inverted cantilever beams on carts with tip masses [8], [9]. In [10] and [11], a pendulum is free to rotate at a pivot on a moving cart. Singla [12] models a cart-pole system as a series of two rigid rods linked by torsional springs.

To model the dynamics of the soft appendage we employ a planar discrete elastic rod (PDER) formulation in state-space

form [6]. We first design a full-state feedback controller for the system linearized about the upwards vertical equilibrium and apply that controller to simulations of the full nonlinear system. We then design a linear observer using a standard Kalman filter design and stabilize the up equilibrium using observer-based feedback with only one angle measurement collected at the base of the appendage only.

The contributions of this paper are (1) a state-space description of a soft swinging appendage with torque input using planar discrete elastic rod theory; (2) a state-feedback control design for balancing the soft appendage in an unstable vertical configuration; and (3) a dynamic output-feedback control design using a linear observer that relies only on measurements of the orientation of the base of the rod. Performance is illustrated using numerical simulations of the nonlinear system and hardware experiments using a silicone rubber appendage. The parameters of the hardware system are chosen to satisfy the conventional self-buckling condition; simulations suggest that the feedback control design balances some appendages that would otherwise buckle under their own weight even with the base angle fixed.

The outline of the paper is as follows. Section II derives the nonlinear mathematical model. Section III presents a feedback control design based on the model linearized about the unstable equilibrium. Section IV presents experimental data and discuss system performance. Finally, Section V summarizes the results and ongoing work.

II. NONLINEAR MATHEMATICAL MODEL

A soft appendage is a continuum structure with an infinite number of degrees of freedom [9]. In order to characterize the behavior of a soft appendage, we utilize a discrete model of an elastic rod. The behavior of the elastic rod is suitably approximated using a planar discrete elastic rod formulation (PDER) [6], which is a specialization of three-dimensional discrete elastic rod theory [13], [14]. The rod is discretized into a series of $N + 1$ nodes (labeled 0 to N) and N edges (labeled 1 to N). The more nodes, the more closely the PDER agrees with analytical models [14].

For our derivation of the PDER equations of motion, we follow the conventions of [6]. The position of the k^{th} node is $\mathbf{x}_k = x_k \mathbf{E}_1 + y_k \mathbf{E}_2$, where x_k and y_k are Cartesian coordinates, \mathbf{E}_1 is a unit vector in the horizontal direction, and \mathbf{E}_2 is a unit vector in the vertical direction. It follows that $\mathbf{E}_3 = \mathbf{E}_1 \times \mathbf{E}_2$ is directed out of the plane. Edge vectors $\mathbf{e}^k = \mathbf{x}_k - \mathbf{x}_{k-1}$ connect neighboring nodes, and have associated unit tangent and normal vectors,

$$\mathbf{t}^k = \frac{\mathbf{e}^k}{\|\mathbf{e}^k\|}, \quad \text{and} \quad \mathbf{n}^k = \mathbf{E}_3 \times \mathbf{t}^k, \quad (1)$$

¹Travis Burch is a former graduate student in the Department of Aerospace Engineering at the University of Maryland, College Park, MD, 20742, USA. trburch@umd.edu

²John P. Lathrop is an undergraduate student in the Department of Mechanical Engineering at the University of Maryland, College Park, MD, 20742, USA. jlathrop@umd.edu

³William L. Scott is a postdoctoral research associate in the Department of Aerospace Engineering at the University of Maryland, College Park, MD, 20742, USA. wlscott@umd.edu

⁴Derek A. Paley is the Willis H. Young Jr. Professor of Aerospace Engineering Education in the Department of Aerospace Engineering and the Institute for Systems Research, University of Maryland, College Park, MD, 20742, USA. dpaley@umd.edu

respectively. The discrete curvature κ_k of the rod at internal node k is defined in terms of the signed turning angle $\varphi_k = \theta_{k+1} - \theta_k$ formed as follows between the neighboring edges:

$$\kappa_k = \frac{2 \sin(\varphi_k)}{1 + \cos(\varphi_k)} = 2 \tan\left(\frac{\varphi_k}{2}\right), \quad (2)$$

where $\cos \varphi_k = \mathbf{t}^{k-1} \cdot \mathbf{t}^k$ and $\sin \varphi_k = \mathbf{n}^{k-1} \cdot \mathbf{t}^k$, for $k = 1, \dots, N-1$.

The resting shape of a PDER is defined by the set of intrinsic lengths \bar{l}^i of each edge and intrinsic curvatures $\bar{\kappa}_i$ at each node. Assume a naturally straight rod with $\bar{\kappa}_i = 0$ for all nodes and evenly spaced nodes with $\bar{l}^i = l$ for all edges. Consider a flexible rod of rectangular cross section and uniform density, with total length L_{tot} , density ρ , thickness h , and width w (out of the plane in the E_3 direction). The intrinsic length of each edge is thus $l = L_{tot}/N$ and the mass of each edge is $m = \rho whl$. The mass m_k associated with the k^{th} node is the average mass of the edges meeting at this node, i.e., $m_0 = m_N = m/2$ and $m_k = m$ for $k = 1, \dots, N-1$.

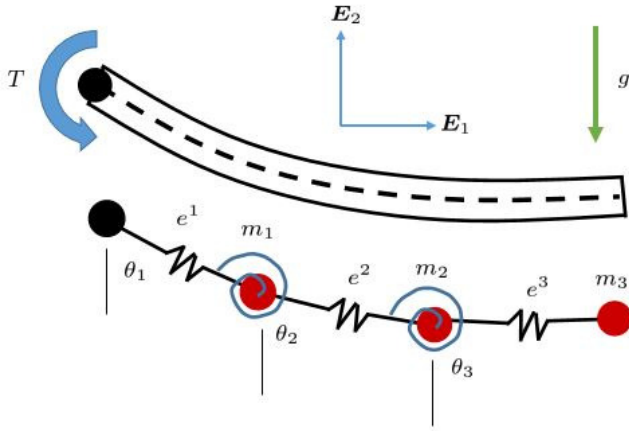


Fig. 1. The PDER model represents a continuous flexible rod as a chain of point mass nodes connected by edges. Edges are modeled as linear elastic springs and nodes are modeled as nonlinear elastic torsional springs. The input to the system is a torque at the base of the appendage.

The PDER dynamics incorporate the various forms of potential energy within the system as follows. The curvatures κ_k determine the elastic bending energy E_b . The change in length of each edge determines the elastic stretching energy E_s . The elastic energies together with the gravitational potential energy E_g form the total potential energy,

$$E_t = E_s + E_b + E_g, \quad (3)$$

with [6]

$$\begin{aligned} E_s &= \frac{1}{2} \sum_{k=1}^N EA \bar{l}^k \left(\frac{\|\mathbf{e}^k\|}{\bar{l}^k} - 1 \right)^2 \\ E_b &= \frac{1}{2} \sum_{j=1}^{N-1} \frac{EI}{\bar{l}^j} (\kappa_j - \bar{\kappa}_j)^2 \\ E_g &= g \sum_{i=0}^N m_i y_i, \end{aligned} \quad (4)$$

where E is the elastic modulus of the rod, $A = wh$ is the cross-sectional area of the rod, and $I = \frac{1}{12} wh^3$ is the area moment of inertia of the rod.

To write the dynamics in state-space form, let $\mathbf{q} = [x_0 \ y_0 \ \dots \ x_{N-1} \ y_{N-1}]^T$ represent the Cartesian coordinates of all of the nodes. The state-space model of the PDER is [6]

$$\begin{aligned} \ddot{x}_k &= -\frac{1}{m_k} \left(\frac{\partial E_t}{\partial x_k} + \mathbf{F}_{x_k} \right) \\ \ddot{y}_k &= -\frac{1}{m_k} \left(\frac{\partial E_t}{\partial y_k} + \mathbf{F}_{y_k} \right), \end{aligned} \quad (5)$$

where \mathbf{F}_{x_k} and \mathbf{F}_{y_k} are the components of all external forces acting on the nodes. For the swinging rod considered here with node 0 fixed in place, the only external (non-conservative) forces are the forces of constraint acting at node 0 and the forces at node 1 that produce the input torque. The stretching, bending, and gravitational forces at each node are conservative and arise from the partial derivative with respect to \mathbf{q} of the corresponding potential energy. For an additional description of these forces refer to [14].

An alternative discretized rod approach was presented in [15]. It is similar to DER except that it uses a definition of curvature that is proportional to the turning angle. At small deformations the models behave similarly, but the model in [15] has bounded curvature (and thus bounded elastic forces), whereas $\kappa_i \in \mathbb{R}$ for the PDER used here.

TABLE I
APPENDAGE PARAMETER VALUES

Name	Parameter	Value	Units
Number of edges	N	5	
Gravitational accel.	g	9.81	$[\frac{m}{s^2}]$
Total length	L_{tot}	0.155	[m]
Rod width	w	0.06	[m]
Rod thickness	h	0.01	[m]
Density	ρ	1.08×10^3	$[\frac{kg}{m^3}]$
Elastic Modulus	E	5.93×10^5	[Pa]
Damping coefficient	d	0.001	

A. Inextensible Rod State-Space Form

Although the PDER model provides a suitable approximation to the elastic rod, for the purposes of control design we further simplify the appendage model as a multi-link rod with inextensible links and nonlinear torsional springs at the nodes. The edge length of the multi-link rod is constant, i.e., $\|\mathbf{e}^i\| = \|\bar{\mathbf{e}}^i\| = l^i$, where l^i is the length of the i^{th} link. The equations of motion for the inextensible nonlinear model are found using the PDER potential energy (3), neglecting the stretching energy, which we find to be one or more orders of magnitude smaller than the bending energy in simulations.

The equations of motion for the inextensible elastic rod follow a recursive pattern that allows the equations to be written for any number of nodes. To incorporate the constant edge-length constraints, it is convenient to describe the system in polar coordinates corresponding to the absolute orientation of each edge. In order to convert from the PDER

state vector (\mathbf{q}, \mathbf{v}) to the state vector of the inextensible model, define $\boldsymbol{\theta} = [\theta_1, \dots, \theta_N]^T$ and $\dot{\boldsymbol{\theta}} = [\dot{\theta}_1, \dots, \dot{\theta}_N]^T$, where

$$\begin{aligned}\theta_i &= \tan^{-1} \left(-\frac{x_i - x_{i-1}}{y_i - y_{i-1}} \right), \\ \dot{\theta}_i &= \frac{\dot{x}_i - \dot{x}_{i-1}}{\|e_i\|} \cos \theta_i + \frac{\dot{y}_i - \dot{y}_{i-1}}{\|e_i\|} \sin \theta_i,\end{aligned}\quad (6)$$

for $i = 1, \dots, N$.

The Euler-Lagrange formulation of (5) yields the following equations of motion:

$$\begin{aligned}\ddot{\boldsymbol{\theta}} &= -\mathcal{M}^{-1}(\boldsymbol{\theta}) \left(\mathcal{C}(\boldsymbol{\theta}, \dot{\boldsymbol{\theta}}) + \mathcal{V}(\boldsymbol{\theta}) + \mathcal{D}(\dot{\boldsymbol{\theta}}) - \mathcal{F}(T) \right) \\ &= h(\boldsymbol{\theta}, \dot{\boldsymbol{\theta}}, T),\end{aligned}\quad (7)$$

where T is the torque input at the base of the rod. The terms \mathcal{M} , \mathcal{C} , \mathcal{V} , and \mathcal{F} in (7) generalize to N links in the following form:

$$\begin{aligned}\mathcal{M}_{ij} &= l^i l^j \cos(\theta_i - \theta_j) \sum_{k=\max\{i,j\}}^N m_k \\ &= ml^2 \cos(\theta_i - \theta_j) \left(n + \frac{1}{2} - \max\{i, j\} \right),\end{aligned}\quad (8)$$

$$\begin{aligned}\mathcal{C}_i &= \sum_{j=1}^N \left[l^i l^j \dot{\theta}_j^2 \sin(\theta_i - \theta_j) \sum_{k=\max\{i,j\}}^N m_k \right] \\ &= ml^2 \sum_{j=1}^N \dot{\theta}_j^2 \sin(\theta_i - \theta_j) \left(n + \frac{1}{2} - \max\{i, j\} \right),\end{aligned}\quad (9)$$

$$\begin{aligned}\mathcal{V}_1 &= \frac{2EI}{l} \left(\bar{\kappa}_1 - \tan\left(\frac{\theta_2 - \theta_1}{2}\right) \right) \sec^2\left(\frac{\theta_2 - \theta_1}{2}\right) \\ &\quad + (N - \frac{1}{2}) mgl \sin(\theta_1), \\ \mathcal{V}_i &= \frac{2EI}{l} \left(\bar{\kappa}_i - \tan\left(\frac{\theta_{i+1} - \theta_i}{2}\right) \right) \sec^2\left(\frac{\theta_{i+1} - \theta_i}{2}\right) \\ &\quad - \frac{2EI}{l} \left(\bar{\kappa}_{i-1} - \tan\left(\frac{\theta_i - \theta_{i-1}}{2}\right) \right) \sec^2\left(\frac{\theta_i - \theta_{i-1}}{2}\right) \\ &\quad + (N - i + \frac{1}{2}) mgl \sin(\theta_1), \quad \text{for } i=2, \dots, N-1, \\ \mathcal{V}_N &= -\frac{2EI}{l} \left(\bar{\kappa}_{N-1} - \tan\left(\frac{\theta_N - \theta_{N-1}}{2}\right) \right) \sec^2\left(\frac{\theta_N - \theta_{N-1}}{2}\right) \\ &\quad + \frac{1}{2} mgl \sin(\theta_1),\end{aligned}\quad (10)$$

$$\begin{aligned}\mathcal{D}_1 &= -d(\dot{\theta}_2 - \dot{\theta}_1) \\ \mathcal{D}_i &= d(-\dot{\theta}_{i-1} + 2\dot{\theta}_i - \dot{\theta}_{i+1}), \quad i = 2, \dots, n, \\ \mathcal{D}_n &= d(\dot{\theta}_n - \dot{\theta}_{n-1}),\end{aligned}\quad (11)$$

for damping coefficient d , and

$$\mathcal{F} = [T \ 0 \ \dots \ 0]^T. \quad (12)$$

Let $\mathbf{q}_\theta = [\boldsymbol{\theta} \ \dot{\boldsymbol{\theta}}]^T$. The first-order state-space representation of the inextensible rod dynamics is

$$\dot{\mathbf{q}}_\theta = f(\boldsymbol{\theta}, \dot{\boldsymbol{\theta}}, T) = \begin{bmatrix} \dot{\boldsymbol{\theta}} \\ h(\boldsymbol{\theta}, \dot{\boldsymbol{\theta}}, T) \end{bmatrix}, \quad (13)$$

where $h(\boldsymbol{\theta}, \dot{\boldsymbol{\theta}}, T)$ is from (7).

III. FEEDBACK CONTROLLER DESIGN

This section presents a hybrid control design for the flexible appendage that consists of a linear feedback controller near the up equilibrium and an open-loop swing-up controller. The design of the linear controller uses a PDER state-space representation of the inextensible flexible rod. Simulation results show the swing up and stability behavior of the controlled system for rods above and below the self-buckling threshold.

To emphasize the necessity of closed-loop feedback control for the task of balancing a flexible rod, Fig. 2 compares zero input (no control torque applied), clamped base (angle of first edge fixed at $\theta_1 = \pi$), and the full-state feedback controller derived next.

A. Linear Control Design

For the purpose of stabilizing the up equilibrium, (13) is linearized about \mathbf{q}_θ^* such that $\theta_i = \pi$ and $\dot{\theta}_i = 0$ for all i and $T^* = 0$. Define the coordinate transformation $\mathbf{z} = \mathbf{q}_\theta - \mathbf{q}_\theta^*$ and $u = T - T^*$. Linearization about the up equilibrium yields

$$\dot{\mathbf{z}} = \mathbf{A}\mathbf{z} + \mathbf{B}u, \quad (14)$$

where $\mathbf{A} = \left. \frac{\partial f}{\partial \mathbf{q}_\theta} \right|_{(\mathbf{q}_\theta^*, T^*)}$ and $\mathbf{B} = \left. \frac{\partial f}{\partial T} \right|_{(\mathbf{q}_\theta^*, T^*)}$ are

$$\mathbf{A} = \begin{bmatrix} 0_{N \times N} & I_{N \times N} \\ \frac{EI}{ml^3} \mathbf{A}_b + \frac{g}{l} \mathbf{A}_g & \frac{d}{ml^2} \mathbf{A}_b \end{bmatrix} \quad \text{and} \quad \mathbf{B} = \begin{bmatrix} 0_{N \times 1} \\ \frac{1}{ml^2} \\ -\frac{1}{ml^2} \\ 0_{N-2 \times 1} \end{bmatrix}, \quad (15)$$

with banded matrices

$$\mathbf{A}_b = \begin{bmatrix} -2 & 3 & -1 & 0 & \dots & 0 \\ 3 & -6 & 4 & -1 & 0 & \\ -1 & 4 & -6 & 4 & -1 & 0 & \vdots \\ 0 & \ddots & \ddots & \ddots & \ddots & \ddots & 0 \\ \vdots & 0 & -1 & 4 & -6 & 4 & -1 \\ & & 0 & -1 & 4 & -6 & 3 \\ 0 & & \dots & 0 & -1 & 5 & -4 \end{bmatrix} \quad (16)$$

and

$$\mathbf{A}_g = \begin{bmatrix} a_1 & b_1 & 0 & 0 \\ c_1 & \ddots & \ddots & 0 \\ 0 & \ddots & \ddots & b_{N-1} \\ 0 & 0 & c_{N-1} & a_N \end{bmatrix}, \quad (17)$$

having entries $a_1 = N - \frac{1}{2}$, $a_N = \frac{3}{2}$, $a_i = 2(N - i) + 1$ for $i = 2, \dots, N - 1$; $b_i = i - N + \frac{1}{2}$, and $c_i = i - N - \frac{1}{2}$ for $i = 1, \dots, N - 1$.

The rows of matrix \mathbf{A}_b representing the bending dynamics take the form of finite-difference coefficients for the fourth spatial derivative, such that the linearized system may be considered a spatial discretization of the linear Euler-Bernoulli model for deflection of a beam [16].

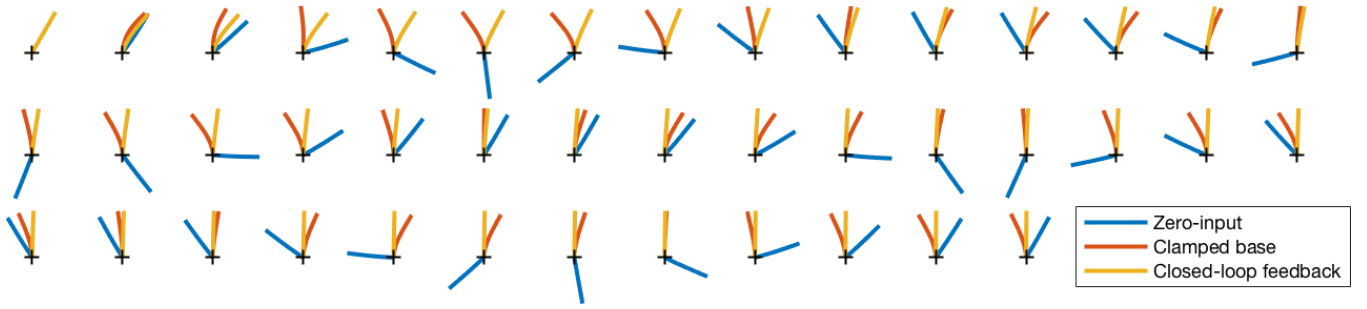


Fig. 2. Snapshots of simulations of the inextensible nonlinear model with $N = 20$ and $L = 12$ cm. Time increases along rows starting from the upper left, showing 2 s in total. Blue: In the zero-input case, the rod acts similar to a rigid pendulum. Red: The first link is clamped at a constant angle $\theta_1 = \pi$ and the rod oscillates about the vertical. Yellow: State feedback control brings the rod to vertical with minimal overshoot, faster than the clamped case.

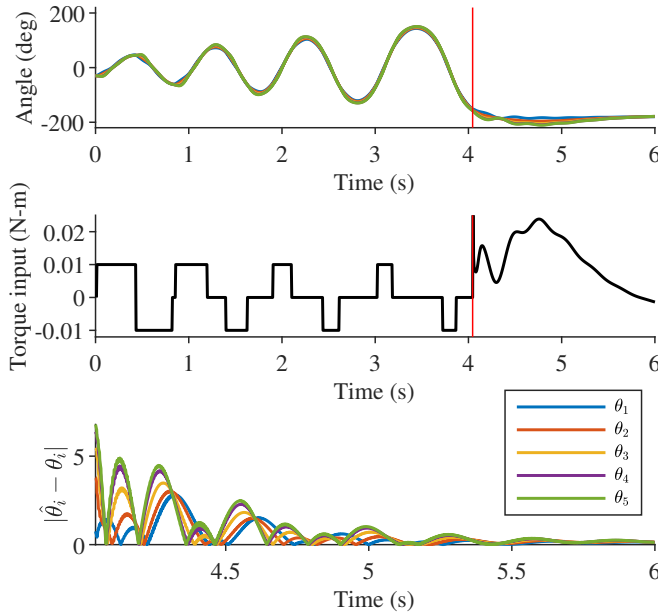


Fig. 3. Simulated swing up and output feedback control performance for system parameter values used in the hardware experiment. Top : Angles over time, with vertical red line denoting the time of switching from swing up to output feedback control. Middle: Torque input over time. Bottom: Error between angles θ_i and estimates $\hat{\theta}_i$ from the time the output feedback control is switched on.

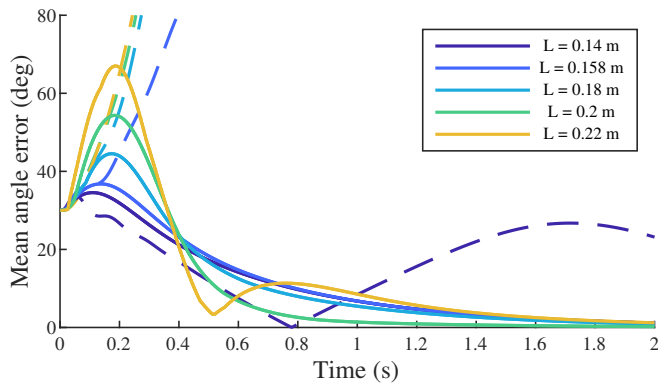


Fig. 4. Simulated full-state feedback control performance of rods below, at, and above the critical self-buckling length of $L_{crit} \approx 0.158$ m. Dashed lines show trajectories with clamped base for comparison. All use $N = 5$ with initial conditions $(\theta_i, \dot{\theta}_i) = (5\pi/6, 0)$ for all i .

The linearized model (14) is used to design a Linear Quadratic Regulator, which minimizes the cost function [17]

$$J = \int_0^{\infty} (z^T Q z + u^T R u) dt, \quad (18)$$

where Q and R are weighting matrices on the state and input, respectively. The feedback control law that minimizes J is $u = -Kz$, where $K = R^{-1}B^T P$. The matrix P is found by solving the continuous time algebraic Riccati equation [17]. In practice, the state-feedback gain matrix K is calculated using the Matlab function `lqr`, with

$$Q = \begin{bmatrix} Q_{\theta} I_{N \times N} & 0_{N \times N} \\ 0_{N \times N} & Q_{\dot{\theta}} I_{N \times N} \end{bmatrix}. \quad (19)$$

For all simulations and experiments presented here, the LQR weights are chosen as $Q_{\theta} = 0.5$, $Q_{\dot{\theta}} = 0.1$, and $R = 1$.

B. Output-Feedback Control

In practice, it is unlikely to have perfect knowledge of the state of the system and more likely to be reliant on information from sensors. Consider a linear output equation $y = Cz$, that maps the state of the system to the signals $y \in \mathbb{R}^M$ measured by the M sensors. In this system, y represents the output of an encoder that measures the angle of the base. The filtered sensor data, in conjunction with the model of the system, yields an estimate of the state using a Luenberger observer [17]:

$$\dot{\hat{z}} = A\hat{z} + Bu + L(y - \hat{y}) \quad (20)$$

where \hat{z} is the estimated state, $\hat{y} = C\hat{z}$ is the estimated output and L is the observer gain matrix such that $A - LC$ is Hurwitz. The C matrix used to design the observer assumes measurements of only the angle of the base of the rod, i.e, the matrix $C \in \mathbb{R}^{1 \times n}$ has all zero entries except $C_{1,1} = 1$, such that $y = \theta_1$. The pair (A, C) is observable. The observer gain matrix L is chosen optimally using the Matlab function `lqr` for the dual system (A^T, C^T) based on weight matrices

$$Q = \begin{bmatrix} 0.05 I_N & 0 \\ 0 & 0.01 I_N \end{bmatrix}, \quad R = 1.$$

Let $e = z - \hat{z}$ be the observer error. Implementing the observer (20) for the linearized state-space system (13) yields

$$\begin{bmatrix} \dot{\hat{z}} \\ \dot{e} \end{bmatrix} = \begin{bmatrix} A - BK & BK \\ 0 & A - LC \end{bmatrix} \begin{bmatrix} \hat{z} \\ e \end{bmatrix}, \quad (21)$$

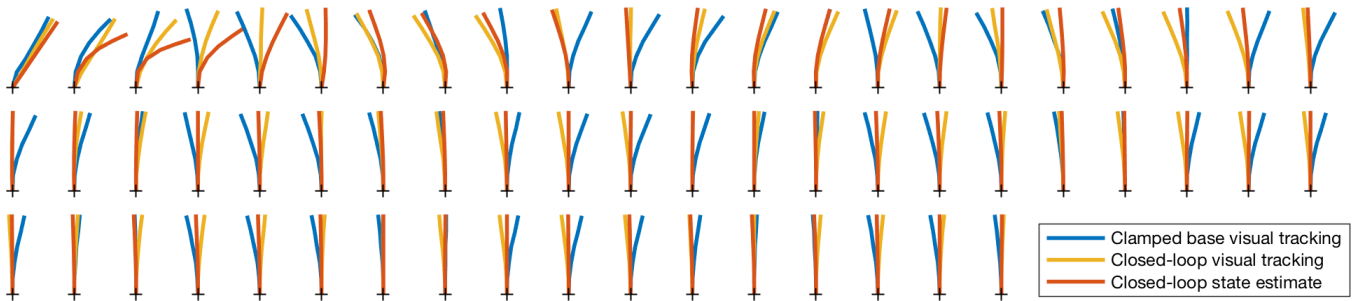


Fig. 5. Experimental performance of output-feedback controller compared to experiment with clamped base. Time increases along rows starting from the upper left, showing three seconds in total. Red: Real-time state estimate based on base angle measurements based on the $N = 5$ linearized model. Yellow: Ground-truth rod shape from visual tracking. Blue: Motion of clamped-end rod from visual tracking.

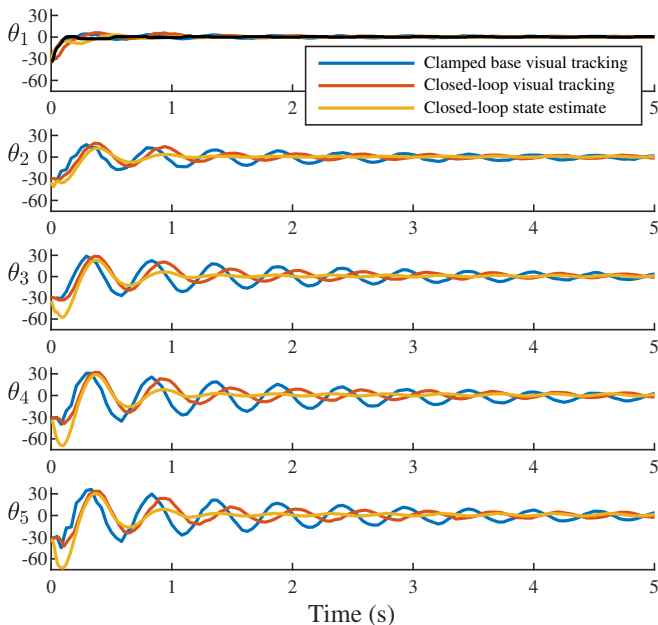


Fig. 6. Experimental performance of output feedback controller compared to clamped base in hardware, plotting the orientation of each edge over time with angles in degrees from vertical. Only θ_1 is measured using the angle sensor for the feedback control (shown as black line).

which is Hurwitz as long as $A - BK$ and $A - LC$ are Hurwitz, i.e., have eigenvalues in the left-half of the complex plane.

C. Swing-up and Hybrid Control Design

We propose a simple swing-up controller to drive the swinging appendage to the effective region of the LQR controller. As the rod swings back and forth across the region of the downward equilibrium, a constant torque is applied in the direction of motion to add energy to the system.

$$u = \begin{cases} u_{swing} \text{sign}(\dot{\theta}_1), & |\theta_i| < \theta_{swing}, \\ 0, & \text{otherwise,} \end{cases} \quad (22)$$

for some chosen amplitude u_{swing} and angle limit θ_{swing} .

Once the base angle θ_1 reaches a threshold value near the up equilibrium, the estimator is initialized and the output feedback control is activated. Figure 3 shows a simulation of the swing-up hybrid control, for a rod with $N = 5$ edges

and material parameters based on the rod in our hardware experiment, from Table I. Here the swing-up region is taken to be $\theta_{swing} = 30^\circ$, amplitude $u_{swing} = 0.01$ N-m, and the output feedback switches on once θ_1 is within 30° of vertical. At that instant in time, we initialize the estimator with the values $\hat{\theta}_i = \theta_1$, $\dot{\hat{\theta}}_i = \dot{\theta}_1$ for $i = 1, \dots, N$.

The problem of stabilizing an inverted flexible appendage becomes more challenging when the appendage is itself inherently unstable. At certain parameter values, an elastic rod is subject to a phenomena known as self-buckling, i.e., it fails to stand under its own weight. A vertical column with base angle clamped and a rectangular cross section of density ρ , Young's modulus E , and thickness h , will buckle above a critical length of [18]

$$L_{crit} = \left(\frac{16Eh^2B^2}{3\rho g} \right)^{\frac{1}{3}}, \quad (23)$$

where g is the acceleration due to gravity and $B \approx 1.866$ is the first zero of the Bessel function of the first kind of order $-1/3$. The analytical buckling expression (23) predicts self buckling for a critical length of $L_{crit} \approx 15.8$ cm, based on the parameters of the 1 cm by 6 cm cross section Dragonskin rod. In simulations, our output feedback controller is able to stabilize rods of lengths at and above the critical buckling length, as shown in Fig. 4.

IV. HARDWARE EXPERIMENTS

To verify the performance of our proposed control design, we built a hardware testbed consisting of a soft appendage cast from Dragonskin 30 silicone rubber attached to the shaft of a 12 V DC motor on a fixed frame. The controller and estimator were implemented on a Teensy 3.5 development board to control the motor through a MAX14870 motor driver. The measured output was taken through the built-in quadrature encoder with 48 counts per revolution attached to the motor. With a gearing ratio of 20.4:1, the total number of counts per revolution of the motor shaft is 979.2. This measurement device provides an angular resolution of 0.368 degrees. The controller test setup is shown in Fig. 7.

The length of the flexible appendage is taken from the center of the DC motor shaft as 15.5 cm. The Dragonskin 30 material has material properties as specified in Table I.

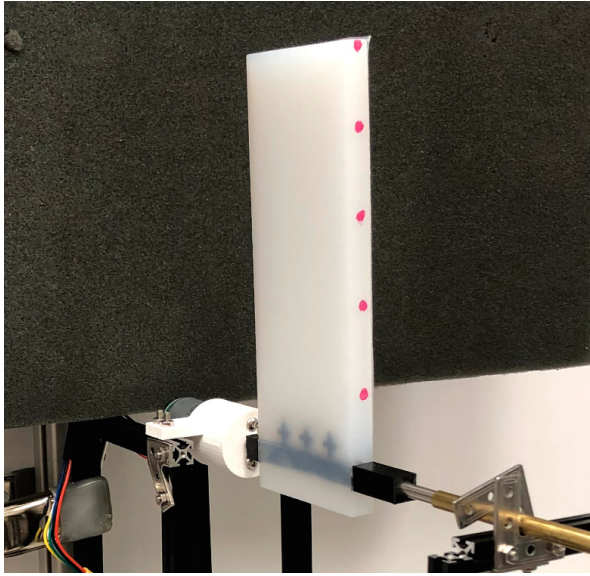


Fig. 7. Experimental setup for the swinging soft appendage, featuring DC motor and Teensy microcontroller. The pink dots are used for visual tracking. In the clamped experiment the base angle is held fixed.

The experiment uses `lqr` controller and estimator weights as described in Sec. III, identical to the simulation.

Comparisons of data from visual tracking and the onboard state estimate from an initial condition of a straight rod at angle $\theta_i = 30^\circ$ are shown in Fig. 5 as snapshots of the shape, and in Fig. 6 as a time series. The experimental controller and estimator stabilize the flexible appendage about the up equilibrium, though some oscillations are present. Visually tracked data for an experiment with clamped end are also included in Figs. 5 and 6, demonstrating that the closed-loop control reaches the upward equilibrium faster with lower amplitude oscillations than an open-loop clamped rod.

The difference between state estimate and visual ground truth in the closed-loop experiment can be primarily attributed to discrepancies between the model and the realized testbed. For example, in the mathematical model used in the controller design, the torque input u is modeled as acting directly on the first edge. In reality, the motor shaft transfers the torque to the base of the rod at the bottom of the first edge. As a result, the behavior of the first edge does not directly follow the PDER model, though this may be improved by including a higher number of nodes in the model. Additionally, the quadrature encoder discretizes the rotation of the appendage to 979.2 counts per revolution. The granular sensor measurement introduces a lack of precision in base link angle, with an angular resolution $\Delta\theta \approx 0.368^\circ$.

V. CONCLUSION

This work provides a state-space description of a swinging flexible appendage based on planar discrete elastic rod theory. State-feedback and output-feedback hybrid controllers stabilize the unstable up equilibrium with measurements taken only at the base of the rod. Simulations suggest that the state-feedback hybrid control and output-feedback

hybrid control designs are successful at swinging up and stabilizing the up equilibrium, even for some rods that would otherwise buckle under their own weight. Ongoing work seeks to upgrade our experimental setup to provide improved estimator convergence.

VI. ACKNOWLEDGEMENTS

The authors would like to thank Alyssa Novelia and Oliver O'Reilly for related discussions. This research was supported by ARO Grant No. W911NF1610244 and ONR Grant No. N00D141612208.

REFERENCES

- [1] D. Sun and J. K. Mills, "Control of a rotating cantilever beam using a torque actuator and a distributed piezoelectric polymer actuator," *Applied Acoustics*, vol. 63, no. 8, pp. 885–899, 2002.
- [2] K. C. Galloway, K. P. Becker, B. Phillips, J. Kirby, S. Licht, D. Tchernov, R. J. Wood, and D. F. Gruber, "Soft robotic grippers for biological sampling on deep reefs," *Soft Robotics*, vol. 3, no. 1, pp. 23–33, 2016.
- [3] F. Zhang, P. Washington, and D. A. Paley, "A flexible, reaction-wheel-driven fish robot: Flow sensing and flow-relative control," in *Proc. American Control Conference*, 2016, pp. 1221–1226.
- [4] S. Kawaji and K. Kanazawa, "Control of double inverted pendulum with elastic joint," in *Proc. IEEE/RSJ International Workshop on Intelligent Robots and Systems*, 1991, pp. 946–951.
- [5] S. K. Dwivedy and P. Eberhard, "Dynamic analysis of flexible manipulators, a literature review," *Mechanism and Machine Theory*, vol. 41, no. 7, pp. 749–777, 2006.
- [6] N. N. Goldberg, X. Huang, C. Majidi, A. Novelia, O. M. O'Reilly, D. A. Paley, and W. L. Scott, "On planar discrete elastic rod models for the locomotion of soft robots," *Soft Robotics*, vol. 6, no. 5, pp. 595–610, 2019.
- [7] S. K. Gorade, P. S. Gandhi, and S. R. Kurode, "Modeling and output feedback control of flexible inverted pendulum on cart," in *Proc. International Conference on Power and Advanced Control Engineering*, 2015, pp. 436–440.
- [8] M. V. Trivedi, R. N. Banavar, and B. M. Maschke, "Modeling of hybrid lumped-distributed parameter mechanical systems with multiple equilibria," in *Proc. 18th IFAC World Congress, Milano, Italy*, vol. 18, no. 1, 2011, pp. 7696–7701.
- [9] O. Patil and P. Gandhi, "On the dynamics and multiple equilibria of an inverted flexible pendulum with tip mass on a cart," *Journal of Dynamic Systems, Measurement, and Control*, vol. 136, no. 4, p. 041017, 2014.
- [10] C. Xu and X. Yu, "Mathematical modeling of elastic inverted pendulum control system," *Journal of Control theory and applications*, vol. 2, no. 3, pp. 281–282, 2004.
- [11] J. Tang and G. Ren, "Modeling and simulation of a flexible inverted pendulum system," *Tsinghua Science & Technology*, vol. 14, no. S2, pp. 22–26, 2009.
- [12] A. Singla, "Vibration suppression of a cart-flexible pole system using a hybrid controller," in *Proc. 1st International and 16th National Conference on Machines and Mechanisms, India*, 2013, pp. 375–382.
- [13] M. Bergou, M. Wardetzky, S. Robinson, B. Audoly, and E. Grinspun, "Discrete elastic rods," *ACM Transactions on Graphics*, vol. 27, no. 3, p. 63, 2008.
- [14] M. K. Jawed, A. Novelia, and O. M. O'Reilly, *A Primer on the Kinematics of Discrete Elastic Rods*. Springer, 2018.
- [15] A. D. Marchese, R. Tedrake, and D. Rus, "Dynamics and trajectory optimization for a soft spatial fluidic elastomer manipulator," *The International Journal of Robotics Research*, vol. 35, no. 8, pp. 1000–1019, 2016.
- [16] J. M. Gere and S. P. Timoshenko, *Mechanics of materials*. PWS-KENT Publishing Company, 1997.
- [17] C.-T. Chen, *Linear system theory and design*. Oxford University Press, 1998.
- [18] A. G. Greenhill, "Determination of the greatest height consistent with stability that a vertical pole or mast can be made, and of the greatest height to which a tree of given proportions can grow," *Proc. Cambridge Philosophical Society*, vol. 4, pp. 65–73, 1881.